Journal of the Taiwan Institute of Chemical Engineers 174 (2025) 106207

Contents lists available at ScienceDirect

Journal of the Taiwan Institute of Chemical Engineers

journal homepage: www.journals.elsevier.com/journal-of-the-taiwan-institute-of-chemical-engineers

Improving dye-sensitized solar cell longevity: An aerogel encapsulation approach

Savisha Mahalingam [a,*], Abreeza Manap [a,*], Kam Sheng Lau [b,*], Dita Floresyona [c], Chin Hua Chia [b], Nurfanizan Afandi [d], Puvaneswaran Chelvanathan [e], Faiz Arith [f,*], Agung Nugroho [c,*]

[a] Institute of Sustainable Energy, Universiti Tenaga Nasional, Jalan IKRAM-UNITEN, 43000 Kajang, Selangor, Malaysia
[b] Materials Science Program, Faculty of Science and Technology, Universiti Kebangsaan Malaysia, 43600 Bangi, Selangor, Malaysia
[c] Department of Chemical Engineering, Faculty of Industrial Technology, Universitas Pertamina, Jalan Teuku Nyak Arief, Simprug, Kebayoran Lama, Jakarta 12220, Indonesia
[d] Department of Mechanical Engineering, College of Engineering, Universiti Tenaga Nasional, Jalan IKRAM-UNITEN, 43000 Kajang, Malaysia
[e] Solar Energy Research Institute (SERI), Universiti Kebangsaan Malaysia, 43600 Bangi, Selangor, Malaysia
[f] Faculty of Electronics and Computer Technology and Engineering, Universiti Teknikal Malaysia Melaka, Hang Tuah Jaya, Durian Tunggal, 76100, Melaka, Malaysia

ARTICLE INFO

Keywords:
Conductivity
Energy
Electrical properties
Heteroatoms

ABSTRACT

The primary challenge in dye-sensitized solar cells (DSSCs) is electrolyte leakage, compromising long-term stability and performance. Alternative electrolytes and encapsulation strategies have been explored to address this. In this study, we propose using nitrogen, fluorine, and sulfur-doped reduced graphene oxide (NSF-rGO) aerogel as an electrolyte encapsulator within DSSCs. The NSF-rGO aerogel was synthesized using a one-pot hydrothermal technique and serves to trap the liquid electrolyte, enhancing cell stability while maintaining conductivity. Although the initial power conversion efficiency of the NSF-rGO-based DSSC was lower than that of the conventional DSSC, it demonstrated significantly improved long-term stability. After two years, the efficiency drop in the NSF-rGO encapsulated DSSC was notably less than in the conventional design, indicating effective electrolyte retention and resistance to degradation. These results suggest that NSF-rGO aerogel encapsulation is a promising strategy for extending the operational lifespan of DSSCs and contributing to more sustainable energy solutions.

1. Introduction

In a dye-sensitized solar cell (DSSC), the electrolyte is crucial in converting light into electrical energy [1,2]. The DSSC consists of several key components: a semiconductor (typically titanium dioxide) coated with a dye, electrodes (typically made of glass coated with a transparent conductive oxide), and an electrolyte. The electrolyte in DSSCs has three main functions: (i) redox mediation, which facilitates the flow of electrons between the dye-sensitized semiconductor and the electrodes. It acts as a redox mediator, helping to transport electrons from the dye to the anode (usually made of platinum) and completing the electrical circuit; (ii) regeneration of dye molecules: the dye molecules on the semiconductor surface absorb light and become excited. The electrolyte helps regenerate these dye molecules by providing electrons to them, allowing the dye to continue absorbing light and contributing to the generation of electric current; (iii) conduction of ions: the electrolyte also aids in the conduction of ions (typically triiodide/iodide ions) between the anode and the cathode. This flow of ions helps maintain charge neutrality within the cell. However, the main limitation of DSSC commercialization is the issues associated with electrolytes [1,2].

Issues and challenges associated with the electrolytes in DSSCs include (i) electrolyte stability: many traditional liquid electrolytes used in DSSCs can be volatile and prone to evaporation. This can lead to decreased efficiency and long-term stability of the solar cell.; (ii) corrosion: the corrosive nature of certain electrolytes can damage the cell components, impacting the durability and overall lifespan of the DSSC; (iii) sealing challenges: liquid electrolytes require proper sealing

* Corresponding authors.
E-mail addresses: savisha@uniten.edu.my (S. Mahalingam), abreeza@uniten.edu.my (A. Manap), kslau@ukm.edu.my (K.S. Lau), faiz.arith@utem.edu.my (F. Arith), agung.n@universitaspertamina.ac.id (A. Nugroho).

https://doi.org/10.1016/j.jtice.2025.106207
Received 4 February 2025; Received in revised form 5 May 2025; Accepted 21 May 2025
Available online 28 May 2025

to prevent leakage and maintain the integrity of the cell. Developing effective and long-lasting seals can be a technical challenge; (iv) sensitivities to temperature: some liquid electrolytes may be sensitive to temperature changes, affecting the performance of the DSSC under varying environmental conditions [3]. Researchers are actively exploring alternative electrolytes, such as solid-state electrolytes or ionic liquids, to address these challenges and enhance the stability and efficiency of DSSCs [3,4]. These alternative electrolytes aim to improve the overall performance and longevity of DSSCs while mitigating issues associated with traditional liquid electrolytes. In this work, we are focusing on using an electrolyte encapsulator/scaffold in DSSC.

An "electrolyte encapsulator" or "scaffold" in a DSSC refers to a structure or material that houses or contains the electrolyte within the cell [5,6]. This encapsulation is crucial for the stability, performance, and longevity of the DSSC. One common approach to encapsulate the liquid electrolyte is using gel electrolytes. Gel electrolytes typically comprise a liquid electrolyte immobilized within a polymer matrix. This gel structure helps to reduce issues related to leakage and evaporation, contributing to the long-term stability of the cell. Solid or quasi-solid polymer electrolytes are another type of encapsulating material. These electrolytes contain both the ionic conductive properties required for the redox reactions in the DSSC and a solid or gel-like structure that helps immobilize the electrolyte [3,5]. Solid-state polymer electrolytes can enhance the stability of the DSSC and reduce issues associated with liquid electrolytes [7]. In addition to the electrolyte-specific encapsulation, other components of the DSSC, such as the semiconductor layer and the dye, may also be encapsulated or protected by layers or coatings. These encapsulation layers can prevent external contaminants from affecting the cell's performance and improve overall durability. The encapsulator or scaffold in a DSSC also contributes to effective sealing, preventing the ingress of moisture and other external elements [3,5]. Proper sealing is critical to maintaining the integrity of the cell over time [8,9].

In this work, reduced graphene oxide (rGO) was doped with heteroatoms such as nitrogen (N), fluorine (F), and sulfur (S) to form an encapsulator layer designed to retain liquid electrolyte [10–12]. Many attempts have been made to increase the electrochemical properties of rGO material, such as doping with heteroatoms of N, S [13], phosphorous (P) [14], boron (B) [15,16], and F [17,18]. Doping rGO with an F atom can also improve the properties of rGO by exhibiting a rich semi-ionic C-F bond, which can affect the electrochemical properties and electrical conductivity of rGO [17,18]. N and S co-doping on rGO leads to better electrochemical properties due to the presence of the N and S group on the rGO surface [19–22]. Another work on nitrogen and fluorine co-doped rGO proves the improvement in unique properties compared to single-atom doped rGO [23]. In dye-sensitized solar cells (DSSCs), aerogels can function as encapsulators or structural matrices that enhance stability and electrolyte retention, contributing to improved performance [24,25].

Aerogels can be employed in DSSCs for enhanced light harvesting [26]. Aerogels can encapsulate the dye-sensitized layer in DSSCs, providing a porous and high-surface-area structure. This can enhance light harvesting capabilities by increasing the surface area for dye adsorption, thereby improving the solar cell's overall efficiency. Aerogels can also be used as electrolyte containment [24]. The electrolyte in DSSCs plays a crucial role in facilitating the transport of charge carriers between the photoanode and counter electrode. Encapsulating the electrolyte with aerogels can help contain and stabilize the electrolyte, preventing leakage and improving the long-term stability of the solar cell. Moreover, aerogels are also used for thermal insulation. Aerogels are known for their excellent thermal insulating properties. Incorporating aerogels in DSSCs can help maintain a more stable operating temperature, prevent overheating, and contribute to the overall stability and efficiency of the solar cell [24,26]. Aerogels can also provide great mechanical support to the delicate components of DSSCs. This is particularly beneficial in ensuring the cell's structural integrity, especially in flexible and lightweight solar cell applications.

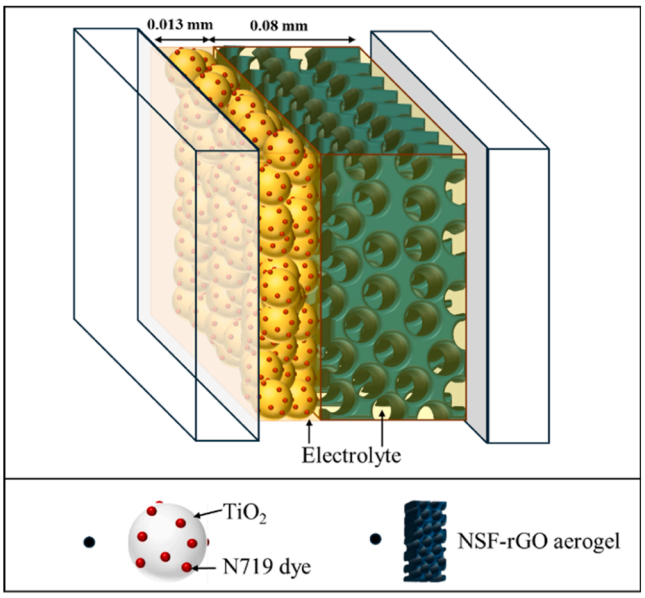

Fig. 1. Schematic diagram of NSF aerogel filled with liquid electrolyte in dye-sensitized solar cell structure.

Here, liquid electrolytes are used because they have the highest conductivity than gel and polymer electrolytes. The study focuses on encapsulating the liquid electrolyte using NSF-rGO and ensuring the electrolyte conductivity is not altered. To our knowledge, using three-heteroatom-doped rGO as an electrolyte encapsulator in DSSCs has not been done before. In this research, we synthesize nitrogen, fluorine, and sulfur co-doped rGO (NSF-rGO) through a simple one-pot hydrothermal technique. Moreover, this work also contributes to the UN Sustainable Development Goals (SDGs) of SDG 7: Affordable and clean energy. The NSF-rGO-based DSSC can be produced with low energy input and is made from non-toxic components.

2. Proposed mechanism

The aerogel's highly porous structure creates a network of interconnected pores. These pores act as tiny reservoirs, trapping and retaining the liquid electrolyte within the aerogel matrix. Capillary forces within the pores help to draw the electrolyte into the aerogel and prevent its leakage or evaporation. The NSF-rGO aerogel is likely functionalized with N, S, and F groups on its surface. These functional groups can interact with the electrolyte molecules through various mechanisms:

- Hydrogen bonding: Nitrogen and sulfur atoms can form hydrogen bonds with the electrolyte molecules [27], creating a stronger association and preventing leakage.
- Ionic interactions: If the electrolyte contains ionic species, the functional groups on the aerogel can interact with them through electrostatic forces, improving electrolyte retention [28].
- Hydrophobic/hydrophilic interactions: The balance of hydrophobic and hydrophilic groups on the aerogel surface can influence the distribution of the electrolyte within the pores [29], optimizing its contact with the electrode surfaces.

N and S atoms within the aerogel structure can create ion-conducting channels [30]. These channels facilitate the movement of ions through the aerogel, enhancing the overall ionic conductivity of the DSSC. The NSF aerogel may also provide electron-transport pathways that facilitate the movement of electrons from the photoanode to the counter electrode. This can enhance the overall efficiency of the DSSC. Overall, the

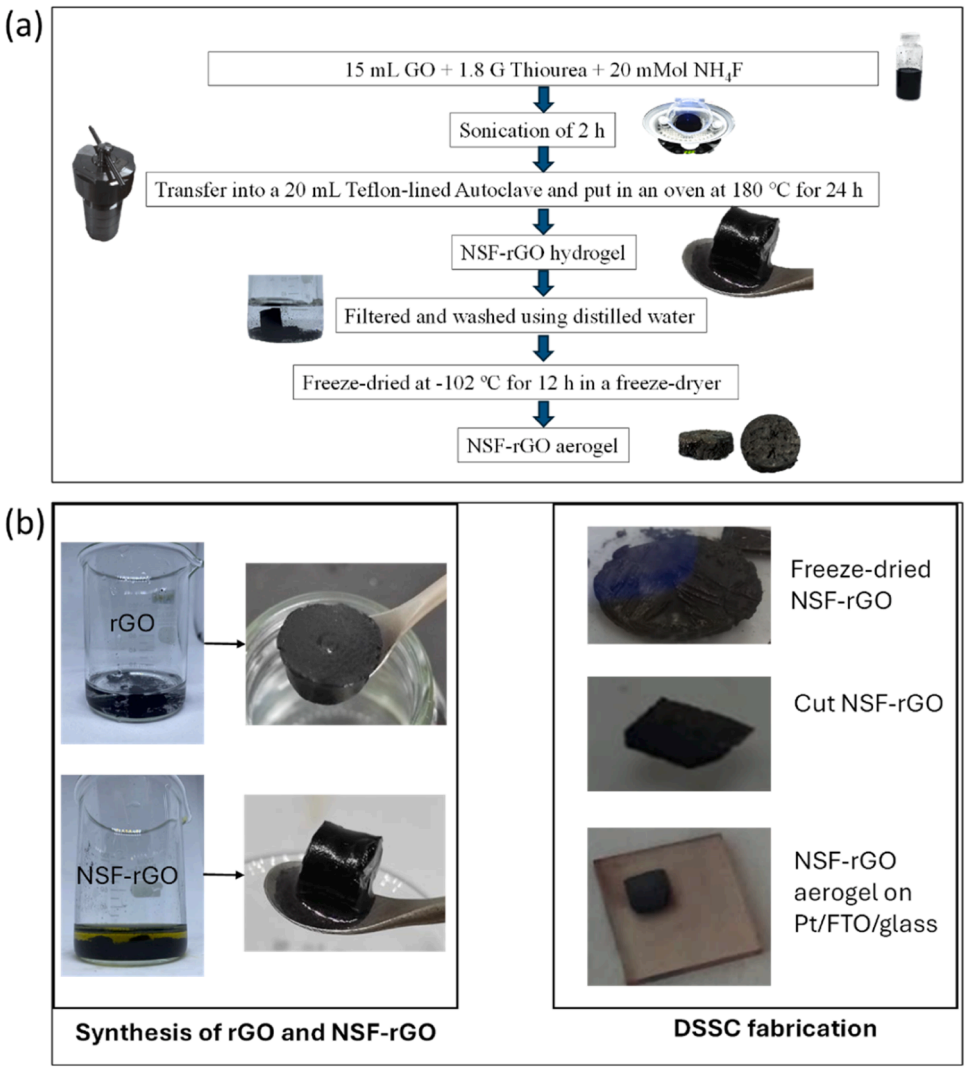

Fig. 2. (a) Flow chart of NSF-rGO aerogel synthesis and (b) prepared NSF-rGO aerogel and NSF-rGO-based DSSC fabrication.

NSF aerogel electrolyte encapsulator in DSSCs is believed to function by physically trapping and retaining the electrolyte, chemically interacting with it, and enhancing ionic conductivity and charge transfer. These mechanisms may contribute to the improved performance and stability of the DSSC. Fig. 1 shows the DSSC structure of NSF aerogel filled with liquid electrolyte. The electrolyte molecules are free to move and diffuse throughout the cell through the pores of the aerogel. This allows for efficient transport of ions between the counter electrode and the photoanode (TiO_2). The liquid electrolyte will indeed diffuse until it covers the entire active layer of the TiO_2. This ensures that the dye molecules can effectively interact with the electrolyte and contribute in the redox reactions required for generating electricity.

3. Methodology

3.1. Synthesis of NSF-rGO aerogel

Graphene oxide was prepared using Modified Hummer's graphite powder method as described in previous research [22,31,32]. A reduced graphene oxide sample was prepared using a hydrothermal method with an autoclave reactor. In this procedure, 15 ml of graphene oxide (GO) suspension was sonicated and transferred into a 20 mL Teflon-lined autoclave. The reaction is held at 180 °C for 24 h before cooling to room temperature. NSF-rGO was synthesized by adding 20 mmol of NH_4F solution containing 600 mg of thiourea into the GO suspension. The suspension was mixed and sonicated for 2 h before hydrothermal treatment. The as-synthesized hydrogel samples underwent a filtration and washing process using distilled water and freeze-dried at −102 °C for 12 h in a freeze dryer to obtain an aerogel. Fig. 2 shows the flow chart of NSF-rGO aerogel synthesis.

3.2. Liquid electrolyte preparation

The triiodide electrolyte solution was prepared by mixing 1 wt. % of iodine and 7.5 wt. % of potassium iodide (SSKI oral solution) in 10 ml of ethylene glycol. The solution was stirred until homogenous and kept in an amber glass vial before use.

3.3. DSSC preparation

The TiO_2 electrodes were prepared using the doctor blade technique on a glass substrate coated with fluorine-doped tin oxide [33]. Di-tetrabutylammonium cis-bis (isothiocyanato) bis (2, 2′-bipyridyl-4, 4′-dicarboxylato) ruthenium (II), referred to as N719 dye, was employed in the immersion process with the annealed TiO_2 thin films for 24 h. A platinum paste was employed for screen-printing the counter electrode, followed by annealing at 400 °C for 1 h. Iodolyte MPN 100 was used as the liquid electrolyte. Simultaneously, the NSF-rGO aerogels were hot

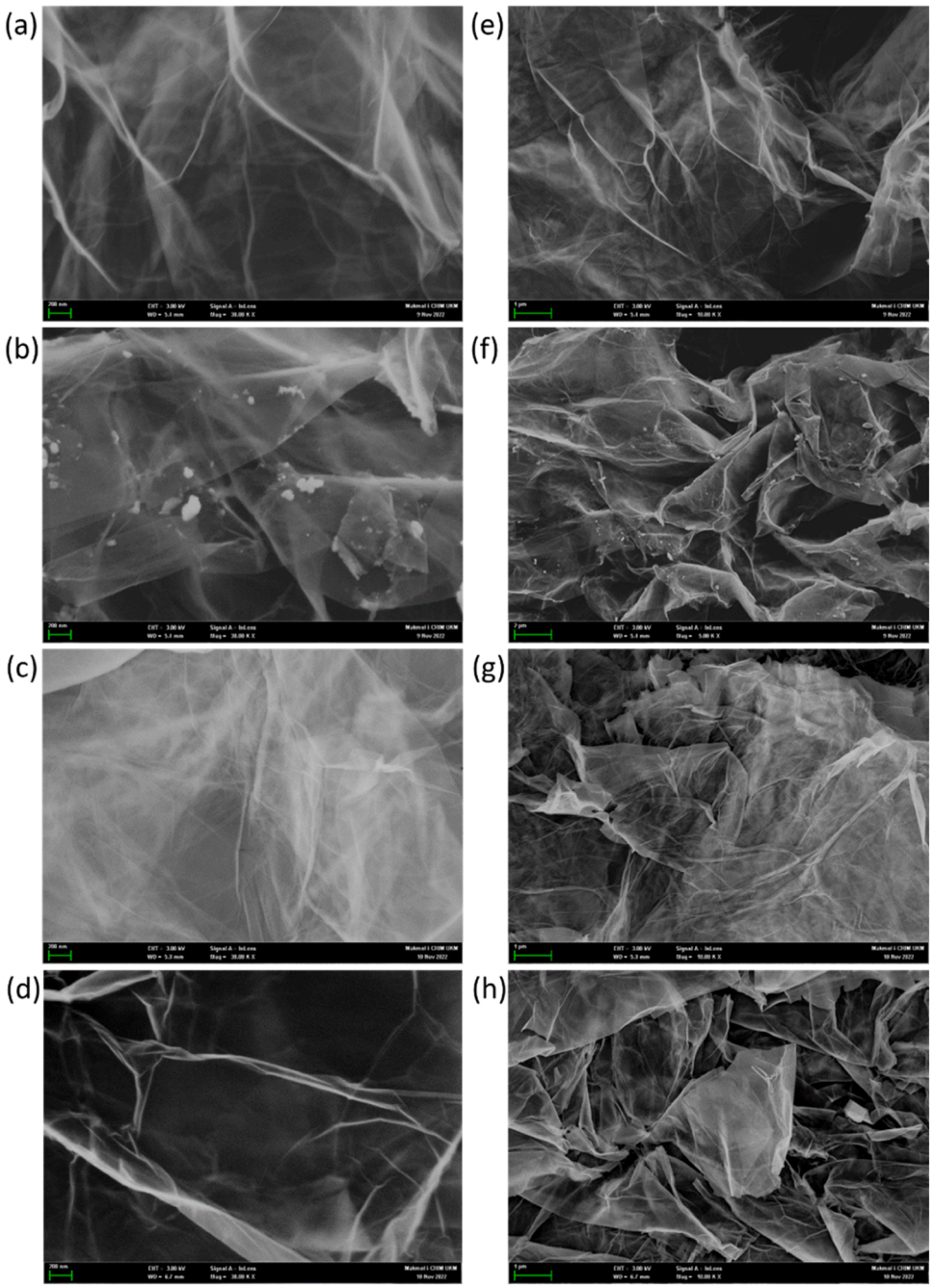

Fig. 3. Morphology from FESEM image at low magnification (a) rGO, (b) N-rGO, (c) NS-rGO, (d) NSF-rGO, and high magnification (e) rGO, (f) N-rGO, (g) NS-rGO, (h) NSF-rGO.

pressed on the platinized FTO and dried at 60 °C for 1 h in an oven. The final thickness of the hot-pressed aerogel was 0.08 mm using a thickness gauge. The hot press was conducted to ensure the sample's thickness will be controlled at 0.08 mm, but in this study, we did not show the optimization of the aerogel thickness. A syringe injected the liquid electrolyte (~30 μL) into the NSF-rGO. The assembly of the DSSC involved sandwiching the dye-immersed TiO_2 and the platinized counter electrode with NSF-rGO. The resulting cell was formed with an active area of 1 cm^2. For result reliability, multiple devices (five DSSCs per case) were prepared.

3.4. Characterizations

The structure and morphology of the rGO and NSF-rGO aerogels were investigated via field emission scanning electron microscopy with energy dispersive X-ray spectroscopy (FESEM-EDX) and high resolution-transmission electron microscopy (HR-TEM). Thesurface chemical was analyzed via X-ray photoelectron spectroscopy (XPS), respectively. The stability of rGO/PET and NSF-rGO/PET with liquid electrolyte was determined using cyclic voltammetry (CV) and electrochemical impedance spectroscopy (EIS). The NSF-rGO aerogel added with 100 μL of triiodide solution was placed in a jig connected to a potentiostat (Gamry, Reference 600). The samples were tested for CV in a potential range of 0 V to 0.8 V at a scan rate of 50 mV/s. EIS measurement was done at a frequency range of 1 MHz to 0.1 Hz. The current density-voltage characteristics and EIS of DSSCs were measured via ORIEL SoI3A Class AAA solar simulator (UNITEN, Malaysia) at air mass and irradiance of 1.5 and 100 mW/cm^2. Current-voltage scan speed and dwell time are 10 mV/

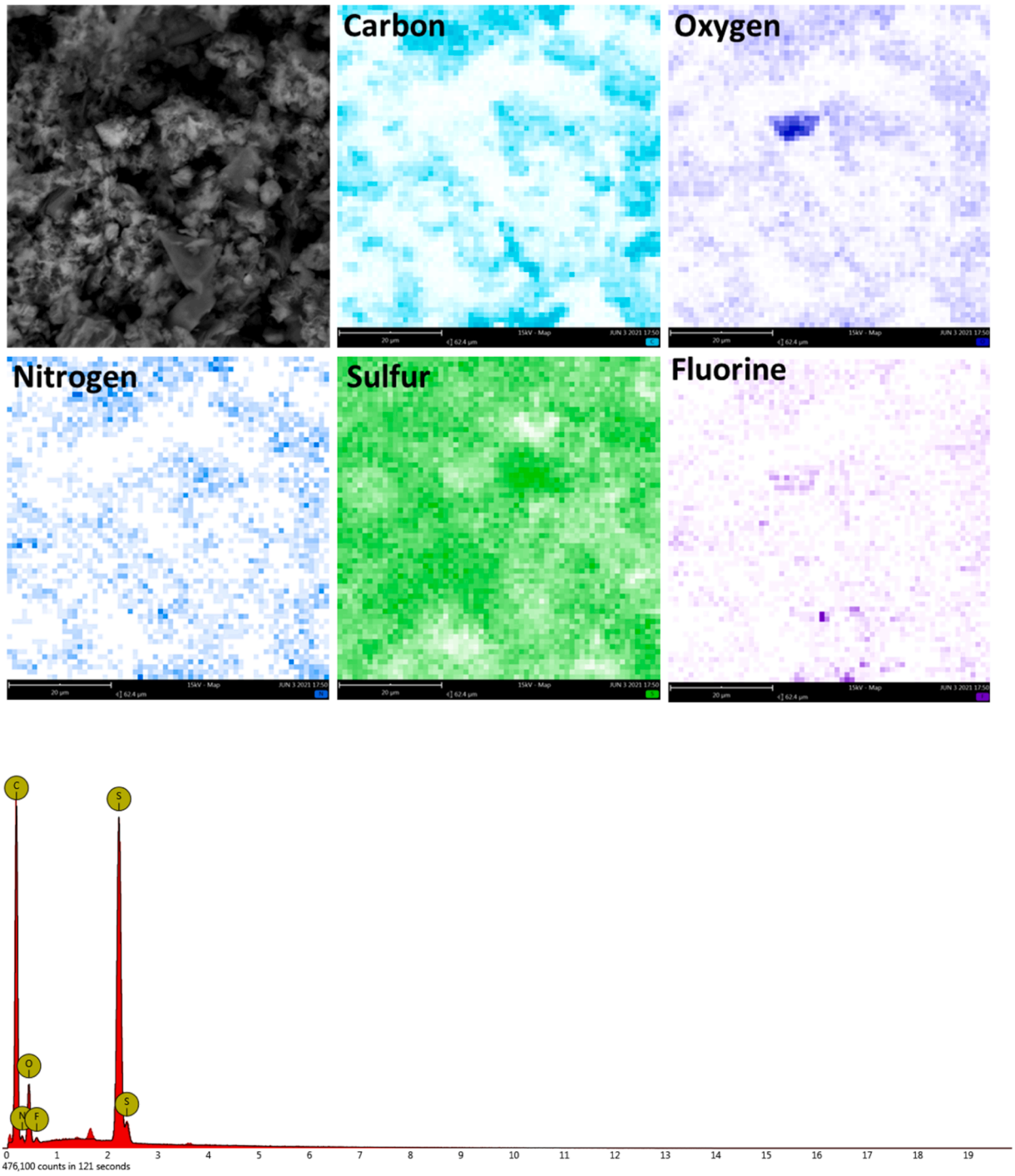

Fig. 4. EDX images NSF-rGO.

steps and 100 ms, respectively. The device illumination area is 5 cm^2, and contact and illumination are determined by masking. This means that the portion of the DSSC that was intentionally exposed to light had a surface area of 5 cm^2 using a mask. The applied voltage and the frequency range for EIS were 0.7 V and 1 MHz to 0.1 Hz, respectively. External quantum efficiency (EQE) determines the efficiency of a solar cell in converting light into electrical current at specific wavelengths utilizing a 2 nm step size (BENTHAM; PVE300-IVT) (Universiti Kebangsaan Malaysia, Malaysia). While photocurrent-time measurements were not performed in this study, the primary focus was to assess long-term device stability over two years through J–V and EQE analysis before and after aging.

4. Results and discussions

4.1. Structure and morphology of aerogels

Fig. 3 shows the morphology analysis of rGO, N-rGO, NS-rGO, and NSF-rGO by FESEM. At a high magnification of 10000x (Fig. 3a-d), the interconnected framework of rGO nanosheets can be seen in all samples. At a low magnification of 30000x (Fig. 3e-h), all samples are composed of very thin rGO sheets. The sheet structure remains rigidly retained after doping atom N or NS, or NSF.

The EDX data shows that rGO mainly comprises C and O, with percentages of 78.9 % and 21.1 %, respectively. By adding NS into the

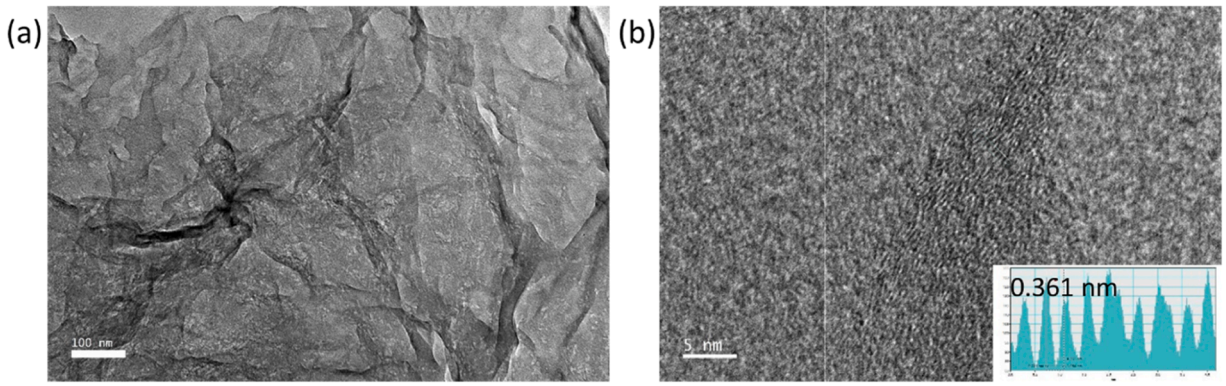

Fig. 5. HR-TEM (a) image of NSF-rGO and (b) lattice fringe.

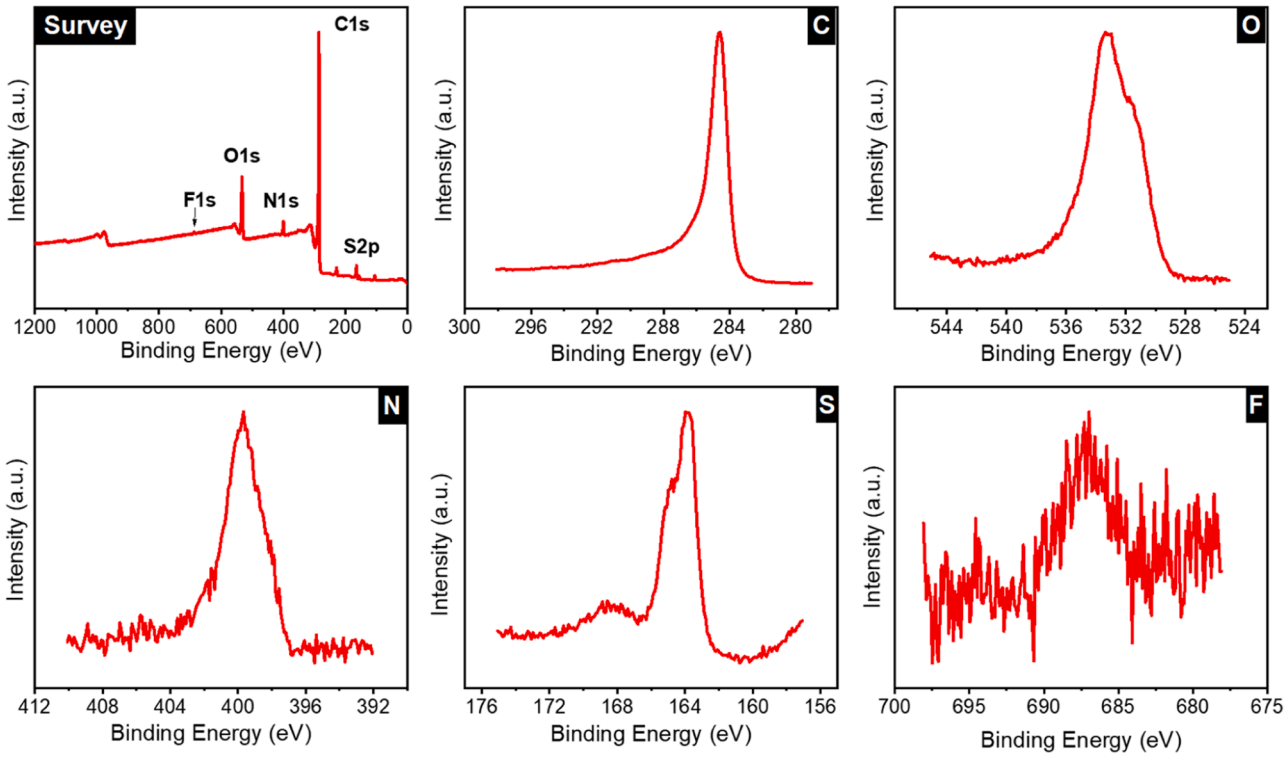

Fig. 6. XPS spectra of NSF-rGO (a) survey, (b) C1s, (c) O1s, (d) N1s, (e) S2p, and (f) F1s.

structure, rGO—NS shows additional NS content with a weight percentage of N (1.67 %) and S (5.24 %) in NS-rGO, respectively. Meanwhile, by adding fluorine into the rGO structure, NSF-rGO has a fluorine weight percentage of 0.62 %. Fig. 4 shows the good distribution of elemental mapping of carbon, nitrogen, and sulfur in the NSF-rGO. The mapping result demonstrates that N, S, and F have been successfully doped into the rGO structure.

Fig. 5 shows the HR-TEM image of NSF-rGO aerogel with lattice fringe. The graphene sheets were visible in Fig. 5a. A lattice fringe of 0.361 nm was obtained. In pure graphene or graphite, the (002) plane (stacking between graphene layers) has a d-spacing ≈ of 0.335 nm [34]. In rGO, the oxygen groups disrupt the structure after partial reduction, increasing the d-spacing [35]. The increased lattice values (> 0.34) obtained in this work are due to the doping with N, S, and F, which further expands or distorts the graphene lattice, leading to even larger d-spacings [34]. Heteroatom doping may create wrinkles, holes, and distortions, slightly varying the interlayer distances [34]. Besides, aerogels are highly porous, the graphene sheets may not stack neatly [36].

4.2. Surface chemical characterization of aerogels

XPS spectra were measured to examine the bond between atoms in rGO—NSF samples (Fig. 6). The XPS survey showed the N, S, and F peaks in 399.8, 163.9, and 686.9 eV, respectively. The N1S spectrum (Fig. 6b) exhibited a slightly broad peak, indicating nitrogen bonding in the structure, which is usually assigned to the pyridine nitrogen or pyrrole group when doping N into carbon materials [37]. In addition to nitrogen, carbonyl, carboxyl, and other oxidized carbons indicated the presence of residual graphene oxide (GO) in rGO—NSF samples. This minor presence of GO is attributed to the incomplete reduction process. Graphitic nitrogen is nitrogen atoms that substitute carbon atoms within the hexagonal graphene ring. In the S2p spectrum (Fig. 6e), two sulfur bonds were identified at 161.44 eV and 162.6 eV, corresponding to -C═S- and C—S—C, respectively. A prominent peak near 168.35 eV was attributed to oxidized sulfur, typically formed at the graphene edges. The first two peaks, at 161.44 eV (2p3/2) and 162.6 eV (2p1/2), are due to spin-orbit coupling in sulfur, representing thiophene. Fig. 6f provides

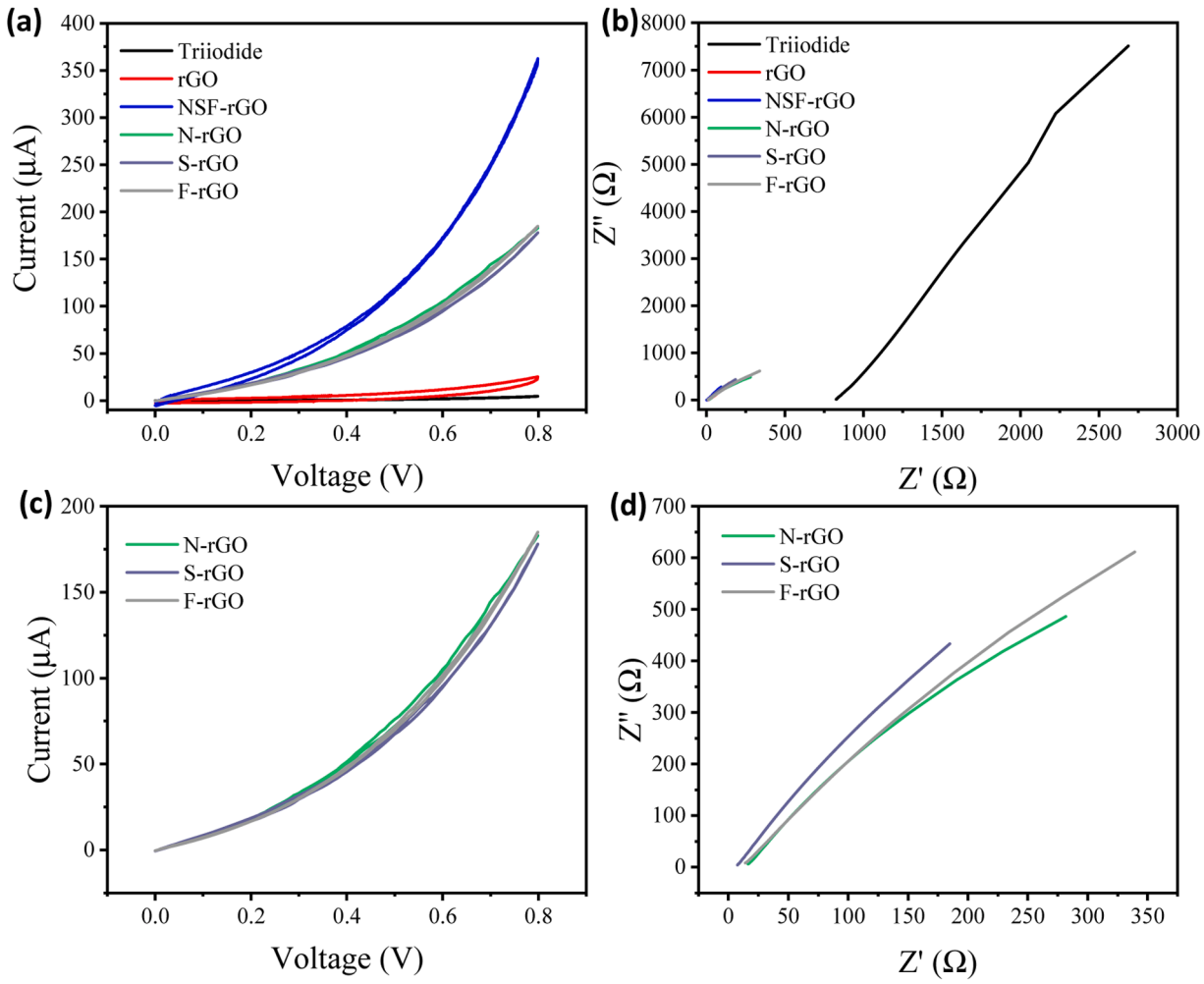

Fig. 7. Triiodide electrolyte solution and triiodide-filled aerogels (rGO, N-rGO, S-rGO, F-rGO, NSF-rGO) of (a) CV, (b) Nyquist spectra, and inset of zoomed graph of (c) CV and (d) Nyquist spectra.

Table 1
Electrode resistance (R_s) and ion charge transfer resistance (R_{ct}) of triiodide electrolyte solution, rGO aerogel, and NSF-rGO aerogel filled with triiodide electrolyte solution.

Sample	R_s (Ω)	R_{ct} (Ω)
Triiodide electrolyte	10.53	492.8
rGO aerogel	2.433	7.428
N-rGO aerogel	0.683	17.31
S-rGO aerogel	0.490	8.02
F-rGO aerogel	0.927	15.33
NSF-rGO aerogel	0.069	4.168

a detailed high-resolution F1s spectrum, confirming fluorine bonding on the surface of the NSF-rGO structure [38].

4.3. CV and EIS of aerogel

The electrochemical stability of the rGO aerogel was investigated using CV and EIS, as shown in Fig. 7. From the CV curves, the presence of the rGO aerogel sample in the triiodide electrolyte solution shows a slight increase in the overall current. In contrast, the NSF-rGO aerogel dramatically increases the overall current. This is because the presence of NSF elements in the rGO surface can promote adequate ion mobility and promote better electrolyte diffusion in the aerogel matrix. The absence of the redox peak of triiodide in this sample could be due to the rGO aerogel undergoing a reduction process that removes the oxygen-containing functional groups that cause the diminished pseudocapacitive behavior, which is essential for redox activity. The redox peaks of rGO are commonly reported in acidic electrolyte [39,40].

Moreover, EIS measurements (Table 1) were conducted to understand the interfacial resistance between the rGO aerogel and the triiodide electrolyte [8]. The electrode resistance (R_s) for the triiodide electrolyte solution, rGO aerogel, NFS-rGO aerogel, N-rGO aerogel, S-rGO aerogel, and F-rGO aerogel were 10.53, 2.433, 0.069, 0.683, 0.490, and 0.927 Ω, respectively. The ion charge transfer resistance (R_{ct}) for the triiodide electrolyte solution, rGO aerogel, NFS-rGO aerogel, N-rGO aerogel, S-rGO aerogel, and F-rGO aerogel were 492.8, 7.428, 4.168, 17.31, 8.02, and 15.33, respectively. The lower R_s and R_{ct} with the presence of rGO aerogel due to its role as a conductive matrix to allow the adequate ionic mobility of the triiodide molecules in the electrolyte solution. When comparing the mono-element hetero-doped rGO aerogel, S-rGO aerogel shows the lower R_s and R_{ct} among N and F elements. This could be due to the higher affinity of sulfur species, which have strong covalent interactions with triiodide molecules. This event stabilizes the triiodide molecules, thus improving charge transfer and reducing recombination [41]. With N, S, and F doping on the rGO surface, the resistance in the aerogel can further decrease due to the increase of active sites that can promote ion diffusion.

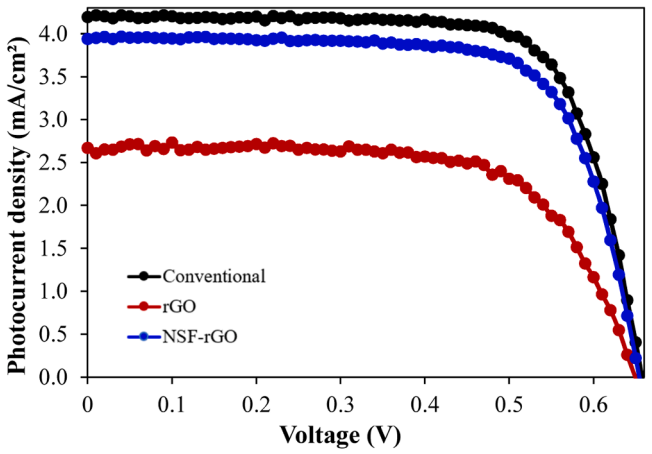

Fig. 8. Photocurrent density-voltage curves of conventional and aerogel-based DSSCs.

Table 2
Photocurrent density-voltage parameters of conventional and aerogel-based DSSCs.

DSSC	J_{sc} (mA/cm^2)	V_{oc} (V)	FF	η (%)
Conventional	4.22 ± 0.02	0.66 ± 0.01	0.74 ± 0.01	2.05 ± 0.02
rGO	2.63 ± 0.04	0.64 ± 0.01	0.68 ± 0.01	1.14 ± 0.02
NSF-rGO	3.85 ± 0.01	0.65 ± 0.01	0.71 ± 0.01	1.77 ± 0.02

4.4. Performance of DSSCs

Fig. 8 provides the J-V curve of conventional DSSC and NSF-based DSSCs. Table 2 tabulates the photovoltaic parameters. The solar power conversion efficiency (η) was obtained using the following equations [42].

$$\eta = \frac{V_{oc} \times J_{sc} \times FF}{P_{in}} \quad (1)$$

$$FF = \frac{V_{\max} \times J_{\max}}{V_{oc} \times J_{sc}} \quad (2)$$

where, V_{oc} is the open circuit voltage at zero current; J_{sc} is the short circuit current at zero voltage; FF fill factor; P_{in} is the incident light power intensity; J_{max} is the maximum current; and V_{max} is the maximum voltage.

While the NSF-aerogel encapsulator exhibits higher ionic conductivity, as evidenced by the CV curves and lower R_{ct} values, the conventional DSSC exhibited higher η than the aerogel encapsulators-based DSSCs. The V_{oc} and FF are almost similar for conventional and aerogel DSSCs. The primary influence is caused by J_{sc}, where the conventional DSSC has the highest J_{sc}. A low J_{sc} can be due to aerogel thickness [43]. Although thickness optimization was not performed in this study, the 0.08 mm thickness was selected based on prior studies [25] demonstrating its suitability for electrolyte retention without significantly hindering DSSC performance. Or et al. reported that thicker aerogels (around 0.044 mm) provide an even distribution of electrolyte components at the photoelectrode [25]. Another reason could be the poor adhesion between the aerogel and the counter electrode, where the aerogel was manually placed on top of the counter electrode and stuck after injecting the electrolyte into the aerogel. Good adhesion is crucial

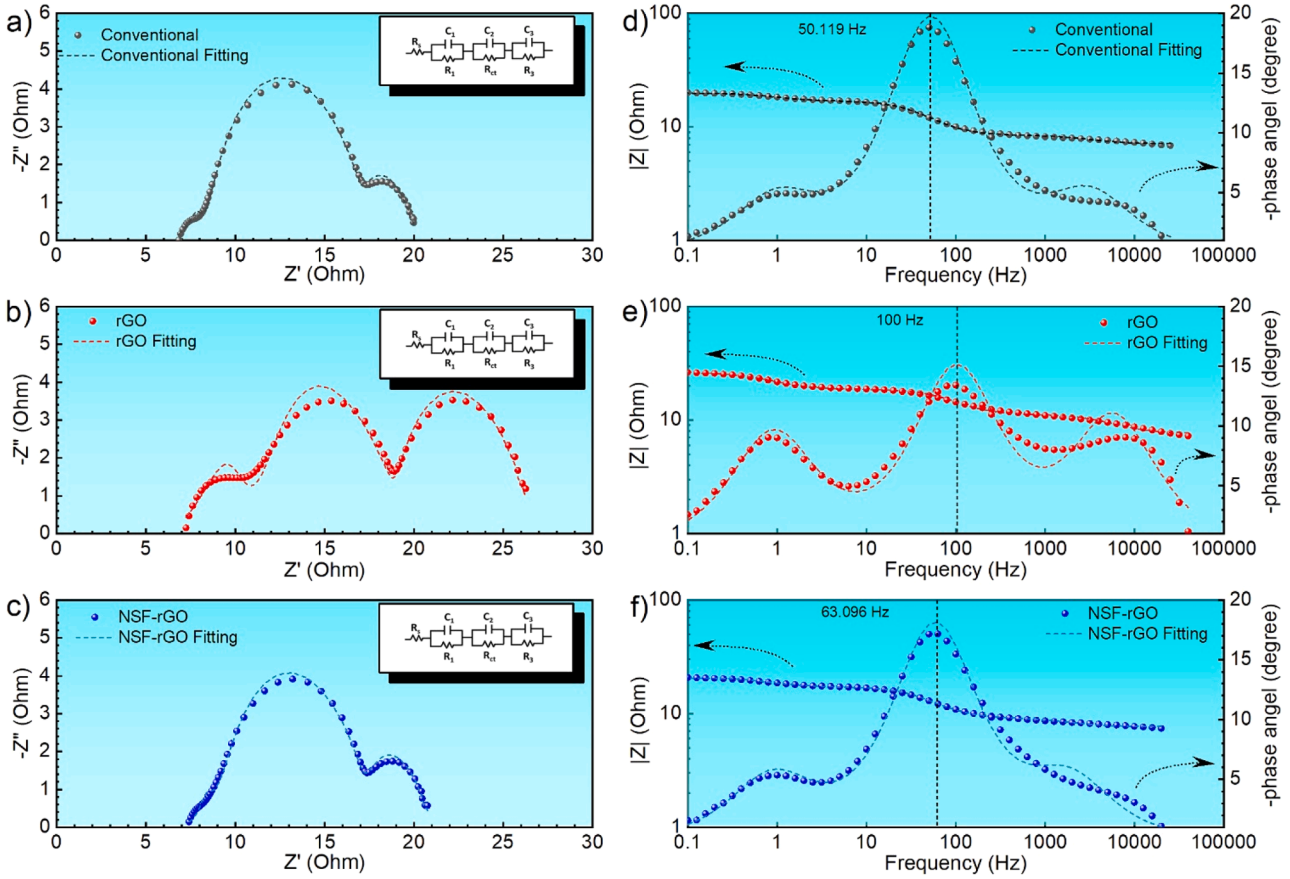

Fig. 9. Nyquist spectra of (a) conventional, (b) rGO, and (c) NSF-rGO DSSCs, and Bode spectra of (d) conventional, (e) rGO, and (f) NSF-rGO DSSCs.

Table 3
Electrochemical impedance spectroscopy parameters of conventional and aerogel-based DSSCs.

DSSC	R_s (Ω)	R_{ct} (Ω)	C_3 (F)	f_{max} (Hz)	τ_{eff} (ms)	k_{eff} (/s)
Conventional	7.13	1.30	0.000506	50.10	3.18	314.47
rGO	7.68	7.56	0.02812	100.00	1.59	628.93
NFS-rGO	7.64	1.43	0.000462	63.10	2.52	396.83

for ensuring efficient charge transfer between the electrolyte and the counter electrode. If there are gaps or voids at the interface, it can hinder the movement of ions and electrons, leading to increased charge transfer resistance and reduced J_{sc} [7].

The efficiency of DSSC (2.08 %) in this work is significantly lower than the current state-of-the-art efficiencies, which have reached over 14 % in optimized systems. However, this research is focused on studying the concept of encapsulation using rGO and doped-rGO materials. It aimed to investigate the effect of the common liquid electrolyte (triiodide) using the encapsulation method to mitigate the main problem in DSSC, which is the electrolyte leakage. Besides, the DSSC fabrication was conducted in a simple material lab with minimal equipment, predominantly self-made, which may have limited the overall efficiency. The fabrication process may have introduced defects or impurities that negatively impacted the device's performance. An EIS study was conducted to investigate other factors that may affect the low J_{sc} in NSF-rGO encapsulator-based DSSC, despite its high ionic conductivity.

4.5. Electron transport of DSSCs

Fig. 9 shows the Nyquist, fitted, and Bode spectra of conventional DSSC and the DSSCs of rGO and NSF-rGO aerogel electrolyte encapsulators. Table 3 lists the corresponding EIS parameters. The Nyquist spectra were fitted with an equivalent circuit model shown in the inset Fig. 9. A good Nyquist spectrum for DSSC consists of three distinguished semicircles [44]: (i) the first semicircle (high-frequency region) represents the counter electrode/electrolyte interface, where C_1 and R_1 correspond to the double-layer capacitance and charge transfer resistance, respectively. (ii) C_2 and R_{ct} reflect the double-layer capacitance and charge transfer resistance at the photoanode/electrolyte interface, describing charge accumulation at the interface. (iii) C_3 and R_3 represent the capacitance and resistance of the electrolyte or the diffuse double layer at the electrode/electrolyte interfaces. Additionally, the electron lifetime (τ_{eff}) and effective rate constant (k_{eff}) are calculated using the following equations [45].

$$\tau_{eff} = \frac{1}{2\pi f_{\max}} \tag{3}$$

$$k_{eff} = \frac{1}{\pi_{eff}} \tag{4}$$

where, f_{max} is the maximum frequency of the EIS spectrum. The electron lifetime refers to the time that photogenerated electrons spend in the semiconductor's conduction band before they are collected at the electrode or recombined with the dye molecules [45].

The Z' intercept at the high-frequency region equals the magnitude of series resistance (R_s), which is the ohmic resistance [46]. The R_s is lower in conventional DSSCs than in aerogel-encapsulated DSSCs. The interfaces between the electrolyte and the electrodes in conventional DSSCs might have lower interfacial resistances due to the absence of the aerogel layer, potentially reducing the overall ohmic resistance [47]. Conventional DSSC also possesses the lowest $R_{ct,}$ which is the main reason for the high J_{sc}. Introducing the aerogel layer can create additional interfacial barriers between the electrolyte and the electrode surfaces. These barriers can hinder the movement of electrons and ions, leading to a higher R_{ct} value in aerogel-encapsulated DSSCs. Besides, a thicker aerogel layer can introduce additional resistance due to the increased distance electrons and ions travel. Poor adhesion between the aerogel and the electrode surfaces can also increase interfacial resistance.

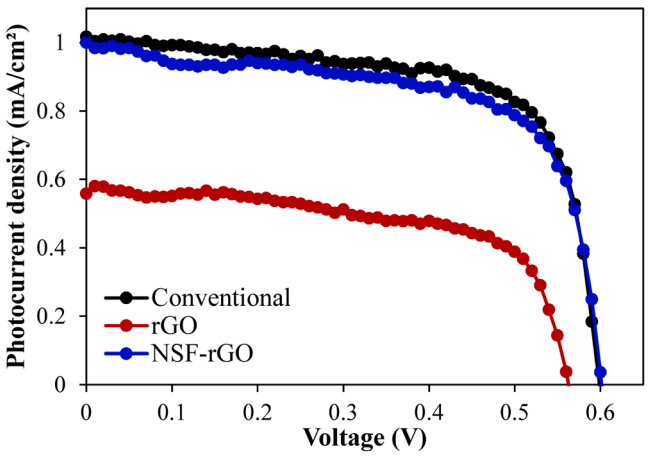

Fig. 10. Photocurrent density-voltage curves of conventional and aerogel-based DSSCs (after two years).

Table 4
Photocurrent density-voltage parameters of conventional and aerogel-based DSSCs (after two years).

DSSC	J_{sc} (mA/cm^2)	V_{oc} (V)	FF	η (%)	Drop in η (%)
Conventional	1.02	0.59	0.68	0.42	80
rGO	0.56	0.56	0.65	0.20	82
NSF-rGO	1.00	0.60	0.66	0.39	78

Meanwhile, rGO aerogel-based DSSC has a higher R_{ct} than NSF-rGO. Introducing N and S functional groups in NSF-rGO aerogels can enhance the interfacial properties between the electrolyte and the electrode surfaces [48]. These functional groups might improve the electron transfer kinetics and reduce the R_{ct} [49]. The previous study suggests that incorporating N and S atoms can alter the electronic properties of the rGO aerogel [50], potentially creating more favorable conditions for electron transfer. Accordingly, the τ_{eff} and k_{eff} follow the same trend as the J_{sc}. Conventional DSSC has the longest τ_{eff} with the least electron recombination rate, followed by NSF-rGO and rGO aerogel. Interestingly, NSF-rGO has the lowest C_3 among the DSSCs. This result shows that although NSF-rGO has a lower η than conventional DSSC, the aerogel can help distribute the electrolyte more uniformly within the DSSC. Additionally, it possesses inherent ionic conductivity properties that can facilitate the movement of ions within the electrolyte, which was also proved in the CV and EIS curves of individual aerogels filled with electrolyte (Fig. 7). Aerogels might influence the diffusion properties of the electrolyte, reducing diffusion limitations. This result confirms that the poor adhesion between the counter electrode and aerogel is the primary reason for the low η in NSF-rGO aerogel, despite the improved electrolyte diffusion due to the additional aerogel layer. While EIS cannot directly quantify physical adhesion, the higher R_{ct} values in the NSF-rGO-based DSSC imply hindered charge transfer, which may result from inadequate aerogel adhesion or interface defects. This interpretation aligns with the observed decrease in J_{sc}.

4.6. Long-term stability (after two years) of DSSCs

After two years, the DSSCs were tested for J-V and EQE, as seen in Fig. 10 and Table 4, and Fig. 11, respectively. The conventional DSSC still exhibited the highest η. The EQE result shows that conventional and NSF-rGO aerogels have similar light absorption at ~520 nm and similar J_{sc} after two years. The drop in η after two years is calculated as (initial

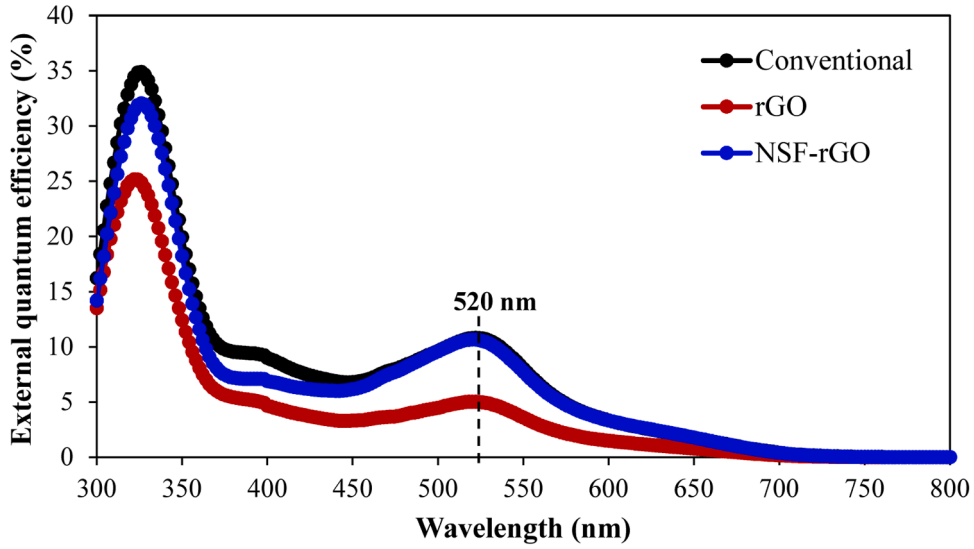

Fig. 11. External quantum efficiency of conventional and aerogel-based DSSCs (after two years).

η-final η)/initial η x 100 %. Although the conventional DSSC exhibited the highest η, NSF-rGO aerogel possessed the lowest drop in η after two years. This event reveals that NSF-rGO aerogel encapsulation has indeed contributed to enhanced long-term stability in the DSSC. These results are not only due to the enhanced ionic conductivity but also other factors such as the porous structure of the aerogel, addditonal functional groups, and improved charge transfer. The porous structure of the aerogel (Figs. 3 and 5) can effectively trap and retain the electrolyte, preventing its leakage and evaporation [25]. This is crucial for maintaining the long-term performance of the DSSC. The functional groups (nitrogen, sulfur, and fluorine) introduced into the rGO structure can improve the aerogel's chemical stability, making it less susceptible to degradation over time [51]. The functional groups in NSF-rGO can also influence the charge transfer kinetics at the electrode/electrolyte interfaces (reduced C_3 as observed in Table 4). By creating favorable conditions for electron and ion transport, NSF-rGO can improve long-term performance [52].

5. Conclusion

This study summarizes that although NSF-rGO aerogel has higher ionic conductivity, improving ionic conductivity alone may not be sufficient to maximize DSSC efficiency. Other factors, such as interface quality, adhesion, and thickness control, are essential. While the NSF-rGO aerogel exhibited a lower initial efficiency and J_{sc} (3.86 to ~1 mA/cm^2 after two years) compared to conventional DSSCs, the relative drop in performance was significantly smaller, highlighting superior long-term stability. The conventional DSSC, despite higher initial J_{sc}, experienced a more substantial efficiency decline (~80 %), mainly due to electrolyte leakage and degradation. This emphasizes the utility of this approach: NSF-rGO encapsulation improves electrolyte retention and device longevity, which are critical for real-world applications. Nonetheless, the long-term performance of the NSF-rGO encapsulated DSSC is a key strength; it retained over 75 % of its initial efficiency after two years, unlike the conventional cell, which showed a drastic drop. The observed limitations related to adhesion and thickness are engineering challenges that need to be addressed in future work to raise initial performance without compromising stability. Although photocurrent-time plots were not included, future work will incorporate real-time photocurrent stability measurements to evaluate the transient response and short-term durability of NSF-rGO encapsulated DSSCs under continuous illumination. Moreover, devices based on single-atom-doped rGO (N-, S-, F-rGO) were not fabricated in this study, but their comparative performance will be evaluated in future work to understand the role of each dopant.

CRediT authorship contribution statement

Savisha Mahalingam: Writing – review & editing, Writing – original draft, Methodology, Investigation, Formal analysis, Data curation, Conceptualization. **Abreeza Manap:** Writing – review & editing, Visualization, Supervision, Resources, Project administration, Funding acquisition, Conceptualization. **Kam Sheng Lau:** Writing – original draft, Software, Methodology, Investigation, Formal analysis, Data curation, Conceptualization. **Dita Floresyona:** Writing – original draft, Resources, Methodology, Investigation, Formal analysis, Data curation, Conceptualization. **Chin Hua Chia:** Writing – review & editing, Software, Resources. **Nurfanizan Afandi:** Writing – review & editing, Resources. **Puvaneswaran Chelvanathan:** Resources, Formal analysis. **Faiz Arith:** Formal analysis, Resources. **Agung Nugroho:** Writing – review & editing, Writing – original draft, Resources, Methodology, Investigation, Formal analysis, Data curation, Conceptualization.

Declaration of interests

The authors declare that they have no known competing financial interests or personal relationships that could have appeared to influence the work reported in this paper.

Acknowledgment

This work was supported by Yayasan Canselor Uniten, Universitas Pertamina-Universiti Tenaga Nasional under the project code of 2020001YCUPU.

References

[1] Wu J, et al. Electrolytes in dye-sensitized solar cells. Chem Rev 2015;115(5):2136–73. https://doi.org/10.1021/cr400675m.
[2] Rahman S, et al. Research on dye sensitized solar cells: recent advancement toward the various constituents of dye sensitized solar cells for efficiency enhancement and future prospects. RSC Adv 2023;13(28):19508–29. https://doi.org/10.1039/D3RA00903C.
[3] Ebenezer Anitha A, Dotter M. A review on liquid electrolyte stability issues for commercialization of dye-sensitized solar cells (DSSC). Energies 2023;16(13). https://doi.org/10.3390/en16135129.
[4] Masud, Kim HK. Redox shuttle-based electrolytes for dye-sensitized solar cells: comprehensive guidance, recent progress, and future perspective. ACS Omega 2023;8(7):6139–63. https://doi.org/10.1021/acsomega.2c06843.

[5] Yang J, Min M, Yoon Y, Kim WJ, Kim S, Lee H. Impermeable flexible liquid barrier film for encapsulation of DSSC metal electrodes. Sci Rep 2016;6(1):27422. https://doi.org/10.1038/srep27422.
[6] Martins J, Emami S, Ivanou D, Mendes A. Ultralow temperature glass frit encapsulation for stable dye-sensitized solar cells. ACS Appl Energy Mater 2022;5(11):14185–92. https://doi.org/10.1021/acsaem.2c02714.
[7] Wang N, Hu J, Gao L, Ma T. Current progress in solid-State electrolytes for dye-sensitized solar cells: a mini-review. J Electron Mater 2020;49(12):7085–97. https://doi.org/10.1007/s11664-020-08483-2.
[8] Văduva M, Burlănescu T, Baibarac M. Functionalization of carbon nanotubes and graphene derivatives with conducting polymers and their applications in dye-sensitized solar cells and supercapacitors. Polymers 2024;16(1). https://doi.org/10.3390/polym16010053.
[9] Önen T, Karakuş MÖ, Coşkun R, Çetin H. Reaching stability at DSSCs with new type gel electrolytes. J Photochem Photobiol Chem 2019;385:112082. https://doi.org/10.1016/j.jphotochem.2019.112082.
[10] Pothaya S, Poochai C, Chuminjak Y, Kongthong T, Lomas T, Tuantranont A, Sriprachuabwong C. Boosting the rate capability of heteroatom co-doped graphene-supported Na3V2 (PO4) 3 as cathode material for sodium-ion battery full cell. J Taiwan Inst Chem Eng 2025;168:105917.
[11] Dai YM, Chen YS, Zhu WX, Lin ZW, Tsai MH. In-situ fabrication of Ag nanoparticles decorated magnetic N-doped graphene heterogeneous catalyst for the catalytic reduction of 4-nitrophenol. J Taiwan Inst Chem Eng 2024;163:105524.
[12] Selvakumar K, Arunpandian M, Oh TH, Wang Y, Sadhasivam T, Sadhasivam S, Bahajjaj AA, Swaminathan M. Tungsten, copper and cobalt-single metal atom oxides embedded CeO2-MnO2-rGO nanorods as electrocatalysts for efficient oxygen evolution reaction. J Taiwan Inst Chem Eng 2024;163:105653.
[13] Jeon WS, Kim CH, Wee JH, Kim JH, Kim YA, Yang CM. Sulfur-doping effects on the supercapacitive behavior of porous spherical graphene electrode derived from layered double hydroxide template. Appl Surf Sci 2021;558:149867. https://doi.org/10.1016/j.apsusc.2021.149867.
[14] Guo M, et al. Hydrothermal synthesis of porous phosphorus-doped carbon nanotubes and their use in the oxygen reduction reaction and lithium-sulfur batteries. New Carbon Mater 2016;31(3):352–62. https://doi.org/10.1016/S1872-5805(16)60019-7.
[15] Prabhagar V, Kumar MP, Takahashi C, Kundu S, Narayanan TN, Pattanayak DK. Boron-doped graphene quantum dots: an efficient photoanode for a dye sensitized solar cell. New J Chem 2019;43(36):14313–9. https://doi.org/10.1039/C9NJ00052F.
[16] Thirumal V, Pandurangan A, Jayavel R, Ilangovan R. Synthesis and characterization of boron doped graphene nanosheets for supercapacitor applications. Synth Met 2016;220:524–32. https://doi.org/10.1016/j.synthmet.2016.07.011.
[17] Jin T, Chen J, Wang C, Qian Y, Lu L. Facile synthesis of fluorine-doped graphene aerogel with rich semi-ionic C–F bonds for high-performance supercapacitor application. J Mater Sci 2020;55(26):12103–13. https://doi.org/10.1007/s10853-020-04821-1.
[18] Yan P, et al. Fluorine-doped graphene/nanosized carbide-derived carbon composites for high-performance supercapacitor. Nano 2019;14(8):1–11. https://doi.org/10.1142/S1793292019500991.
[19] Zhang W, et al. N/S co-doped three-dimensional graphene hydrogel for high performance supercapacitor. Electrochim Acta 2018;278:51–60. https://doi.org/10.1016/j.electacta.2018.05.018.
[20] Ouyang Z, et al. Preparation and specific capacitance properties of sulfur, nitrogen Co-doped graphene quantum dots. Nanoscale Res Lett 2019;14(1). https://doi.org/10.1186/s11671-019-3045-4.
[21] Lu Z, Chen Y, Liu Z, Li A, Sun D, Zhuo K. Nitrogen and sulfur co-doped graphene aerogel for high performance supercapacitors. RSC Adv 2018;8(34):18966–71. https://doi.org/10.1039/c8ra01715h.
[22] Nugroho A, et al. Synthesis and characterization NS-reduced graphene oxide hydrogel and its electrochemical properties. Lett Mater 2022;12(2):169–74. https://doi.org/10.22226/2410-3535-2022-2-169-174.
[23] Jiao C, Zhang ZJ, Chen XY. Nitrogen and fluorine dual-doped carbon nanosheets for high-performance supercapacitors. Nano 2019;14(4). https://doi.org/10.1142/S1793292019500425.
[24] Mohan K, Bora A, Roy RS, Nath BC, Dolui SK. Polyaniline nanotube/reduced graphene oxide aerogel as efficient counter electrode for quasi solid state dye sensitized solar cell. Sol Energy 2019;186:360–9. https://doi.org/10.1016/j.solener.2019.05.030.
[25] Or T, Miettunen K, Cranston ED, Moran-Mirabal JM, Vapaavuori J. Cellulose nanocrystal aerogels as electrolyte scaffolds for glass and plastic dye-sensitized solar cells. ACS Appl Energy Mater 2019;2(8):5635–42. https://doi.org/10.1021/acsaem.9b00795.
[26] Gao X-D, et al. Aerogel based SiO2–TiO2 hybrid photoanodes for enhanced light harvesting in dye-sensitized solar cells. J Mater Chem 2012;22(36):18930–8. https://doi.org/10.1039/C2JM33945E.
[27] Ruan C, Xie Y. Electrochemical performance of activated carbon fiber with hydrogen bond-induced high sulfur/nitrogen doping. RSC Adv 2020;10(62):37631–43. https://doi.org/10.1039/D0RA06724E.
[28] Li C, Shi G. Functional gels based on chemically modified graphenes. Adv Mater 2014;26(24):3992–4012. https://doi.org/10.1002/adma.201306104.
[29] Volfkovich YM, et al. Hydrophilic and hydrophobic pores in reduced graphene oxide aerogel. J Porous Mater 2019;26(4):1111–9. https://doi.org/10.1007/s10934-018-0712-2.
[30] Flouda P, Bukharina D, Pierce KJ, Stryutsky AV, Shevchenko VV, Tsukruk VV. Flexible sustained ionogels with ionic hyperbranched polymers for enhanced ion-conduction and energy storage. ACS Appl Mater Interfaces 2022;14(23):27028–39. https://doi.org/10.1021/acsami.2c04502.
[31] Paulchamy B, Arthi G, Lignesh B. A simple approach to stepwise synthesis of graphene oxide nanomaterial. J Nanomed Nanotechnol 2015;06(01):1–4. https://doi.org/10.4172/2157-7439.1000253.
[32] Zaaba NI, Foo KL, Hashim U, Tan SJ, Liu WW, Voon CH. Synthesis of graphene oxide using modified Hummers method: solvent influence. Procedia Eng 2017;184:469–77. https://doi.org/10.1016/j.proeng.2017.04.118.
[33] Agrawal A, Siddiqui SA, Soni A, Khandelwal K, Sharma GD. Performance analysis of TiO2 based dye sensitized solar cell prepared by screen printing and doctor blade deposition techniques. Sol Energy 2021;226:9–19. https://doi.org/10.1016/j.solener.2021.08.001.
[34] He C, Zhang JJ, Shen PK. Nitrogen-self-doped graphene-based non-precious metal catalyst with superior performance to Pt/C catalyst toward oxygen reduction reaction. J Mater Chem A 2014;2(9):3231–6. https://doi.org/10.1039/C3TA14070A.
[35] Sharma N, Sharma V, Sharma SK, Sachdev K. Gas sensing behaviour of green synthesized reduced graphene oxide (rGO) for H2 and NO. Mater Lett 2019;236:444–7. https://doi.org/10.1016/j.matlet.2018.10.145.
[36] Liu P, et al. 3D Lamellar-structured graphene aerogels for thermal interface composites with high through-plane thermal conductivity and fracture toughness. Nano-Micro Lett 2020;13(1):22. https://doi.org/10.1007/s40820-020-00548-5.
[37] Nugroho A, Nursanto EB, Curie CA, Oktaviano HS, Ainurrachma F, Trisunaryanti W. Utilisation of gelatin as nitrogen source for N-doped carbon nanotubes and its performance for the oxygen reduction reaction. Adv Nat Sci Nanosci Nanotechnol 2022;13(3):35004. https://doi.org/10.1088/2043-6262/ac8660.
[38] Guo J, et al. Fluorine-doped graphene with an outstanding electrocatalytic performance for efficient oxygen reduction reaction in alkaline solution. R Soc Open Sci 2018;5(10):180925. https://doi.org/10.1098/rsos.180925.
[39] Hassan HK, Atta NF, Hamed MM, Galal A, Jacob T. Ruthenium nanoparticles-modified reduced graphene prepared by a green method for high-performance supercapacitor application in neutral electrolyte. RSC Adv 2017;7(19):11286–96. https://doi.org/10.1039/C6RA27415C.
[40] Park J, et al. Reduced graphene oxide aerogels with functionalization-mediated disordered stacking for sodium-ion batteries. Batteries 2022;8(2). https://doi.org/10.3390/batteries8020012.
[41] Karthika P, Ganesan S. Poly(ethylene glycol)–poly(propylene glycol)–poly (ethylene glycol) and polyvinylidene fluoride blend doped with oxydianiline-based thiourea derivatives as a novel and modest gel electrolyte system for dye-sensitized solar cell applications. RSC Adv 2020;10(25):14768–77. https://doi.org/10.1039/D0RA01031F.
[42] Giannouli M, Govatsi K, Syrrokostas G, Yannopoulos SN, Leftheriotis G. Factors affecting the power conversion efficiency in ZnO DSSCs: nanowire vs. Nanoparticles. Mater 2018;11(3). https://doi.org/10.3390/ma11030411.
[43] Hamann TW, Martinson ABF, Elam JW, Pellin MJ, Hupp JT. Aerogel templated ZnO dye-sensitized solar cells. Adv Mater 2008;20(8):1560–4. https://doi.org/10.1002/adma.200702781.
[44] Omar A, Ali MS, Rahim NA. Electron transport properties analysis of titanium dioxide dye-sensitized solar cells (TiO2-DSSCs) based natural dyes using electrochemical impedance spectroscopy concept: a review. Sol Energy 2020;207:1088–121. https://doi.org/10.1016/j.solener.2020.07.028.
[45] Bisquert J. Theory of the impedance of electron diffusion and recombination in a thin layer. J Phys Chem B 2002;106(2):325–33. https://doi.org/10.1021/jp011941g.
[46] Bahrami A, Kazeminezhad I, Abdi Y. Pt-Ni/rGO counter electrode: electrocatalytic activity for dye-sensitized solar cell. Superlattices Microstruct 2019;125:125–37. https://doi.org/10.1016/j.spmi.2018.10.026.
[47] Kutlu N. Investigation of electrical values of low-efficiency dye-sensitized solar cells (DSSCs). Energy 2020;199:117222. https://doi.org/10.1016/j.energy.2020.117222.
[48] Jun B-M, et al. Photocatalytic and electrocatalytic degradation of bisphenol A in the presence of graphene/graphene oxide-based nanocatalysts: a review. Chemosphere 2024;356:141941. https://doi.org/10.1016/j.chemosphere.2024.141941.
[49] Ai W, et al. Nitrogen and sulfur codoped graphene: multifunctional electrode materials for high-performance Li-ion batteries and oxygen reduction reaction. Adv Mater 2014;26(35):6186–92. https://doi.org/10.1002/adma.201401427.
[50] Feng Q, et al. Facile synthesis and first-principles study of nitrogen and sulfur dual-doped porous graphene aerogels/natural graphite as anode materials for Li-ion batteries. J Alloys Compd 2021;884:160923. https://doi.org/10.1016/j.jallcom.2021.160923.
[51] Cao L, Wang C, Huang Y. Structure optimization of graphene aerogel-based composites and applications in batteries and supercapacitors. Chem Eng J 2023;454:140094. https://doi.org/10.1016/j.cej.2022.140094.
[52] Prabavathy N, Shalini S, Balasundaraprabhu R, Velauthapillai D, Prasanna S, Muthukumarasamy N. Enhancement in the photostability of natural dyes for dye-sensitized solar cell (DSSC) applications: a review. Int J Energy Res 2017;41(10):1372–96. https://doi.org/10.1002/er.3703.